Published in final edited form as:
Biochemistry. 2013 November 12; 52(45): . doi:10.1021/bi400776z.

New functional aspects of the atypical protein tyrosine phosphatase VHZ

Vyacheslav I. Kuznetsov and **Alvan C. Hengge**
Department of Chemistry and Biochemistry, Utah State University, Logan, UT 84322-0300

Abstract

LDP3 (VHZ) is the smallest classical protein tyrosine phosphatase (PTP) known to date, and was originally misclassified as an atypical dual specificity phosphatase (DSP). Kinetic isotope effects with steady state and pre-steady state kinetics of VHZ and mutants with *para*-nitrophenol phosphate (*p*NPP) have revealed several unusual properties. VHZ is significantly more active than previously reported, but remains one of the least active PTPs. Highly unusual for a PTP, VHZ possesses two acidic residues (E134 and D65) in the active site. D65 occupies the position corresponding to the typical general acid in the PTP family. However, VHZ primarily utilizes E134 as the general acid, with D65 taking over this role when E134 is mutated. This unusual behavior is facilitated by two coexisting, but unequally populated, substrate binding modes. Unlike most classical PTPs, VHZ exhibits phosphotransferase activity. Despite the presence of the Q-loop that normally prevents alcoholysis of the phosphoenzyme intermediate in other classical PTPs, VHZ readily phosphorylates ethylene glycol. Although mutations to Q-loop residues affect this phosphotransferase activity, mutations on the IPD-loop that contains the general acid exert more control over this process. A single P68V substitution on this loop completely abolishes phosphotransferase activity. The ability of native VHZ to catalyze transphosphorylation may lead to an imbalance of intracellular phosphorylation, which could explain the correlation of its overexpression with several types of cancer.

Keywords

Protein-tyrosine phosphatase; dual-specificity phosphatase; PTP; DSP; VHZ

The protein tyrosine phosphatases (PTPs) are a large family of enzymes responsible for intracellular dephosphorylation. Together with protein tyrosine kinases (PTKs), PTPs control the level of protein phosphorylation, which modulates numerous aspects of cell life, such as growth, proliferation, metabolism, intercellular interaction, immune responses, and gene transcription (1). PTPs contain a highly conserved HCXXGXXRS/T signature sequence motif but share very little sequence similarities outside of the conserved regions, which are comprised of the phosphate binding loop (P-loop); the general acid loop, often referred to as the WPD-loop; and the Q-loop that bears conserved glutamine residues that orient the water nucleophile in classical PTPs and prevent phosphotransferase activity to other potential nucleophiles.

To whom correspondence should be addressed: Alvan C. Hengge: alvan.hengge@usu.edu. Phone: (435)797-3442. Fax: (435)797-3390.

Supporting Information is Available. Table of ionization constants associated with catalytically relevant residues; plot of partial extinction coefficients for *p*-nitrophenol versus pH; derivation of equations for PTP-catalyzed reactions in the presence of alternative nucleophiles; and kinetic model including two coexisting substrate binding modes; and a sequence alignment of VHZ, SsoPTP, and Tk-PTP. This material is available free of charge via the Internet at http://pubs.acs.org.

All PTPs utilize a two-step double-displacement mechanism of phosphate monoester hydrolysis (Scheme 1) mediated by an invariant cysteine-arginine-aspartic acid triad of catalytic residues (2). The mechanism proceeds through a phosphoenzyme intermediate where the second chemical step is often rate limiting (3). In the first step the P-loop orients the substrate as the nucleophilic cysteine attacks phosphorus with simultaneous expulsion of the leaving group protonated by the catalytic general acid. In the second step a water molecule, directed by the aspartic acid residue that served as the general acid in the first step and Q-loop glutamine residues, attacks the phosphoenzyme intermediate.

The PTP family is subdivided into several groups based on substrate specificity, subcellular localization, and size. The classical PTP family selectively hydrolyzes phosphotyrosine containing peptides, and includes the well-studied bacterial effector protein YopH, responsible for the virulence of notorious *Y.pestis*, and human PTP1B, which plays an important role in insulin signaling (4). Classical PTPs have a modular organization and, in addition to the catalytic phosphatase domain, contain non-catalytic domains that control subcellular localization and protein-substrate interactions. All classical PTPs are tyrosine specific enzymes. The members of the dual-specificity phosphatases (DSPs) subfamily hydrolyze phosphoserine and phosphothreonine in addition to phosphotyrosine containing target sites. Within the DSP subfamily, the atypical DSPs are smaller and contain only a catalytic domain (5). The classical PTPs and DSPs also differ in their phosphotransferase ability. In classical PTPs the phosphoenzyme intermediate is attacked only by water due to the shielding effect of conserved Q-loop residues, named for the presence of conserved glutamines (6). In contrast, DSPs such as VHR, and the low-molecular weight LMW-Ltp1, both of which lack the Q-loop, display significant phosphotransferase ability (7). On this basis, it has been concluded that the presence of the Q-loop prevents phosphotransferase activity.

VHZ, and the closely related phosphatase *S.solfataricus* PTP (SsoPTP), are among the smallest classical PTPs known to date (Figure 1). The SsoPTP (161 amino acids) is similar to VHZ (150 amino acids) in size and catalytic activity. Both VHZ and SsoPTP consist of a single, catalytic domain that is more similar to classical PTPs than DSPs (8, 9) and contain identical secondary structural elements, but, unlike most classical PTPs, lack an N-terminal extension that forms a substrate recognition/binding loop. Like VHZ, the general acid in SsoPTP resides on a rigid IPD-loop, which, unlike the flexible WPD-loop in classical PTPs, permanently occupies a closed conformation. Unlike VHZ, and like classical PTPs, SsoPTP/WT contains no additional general acid in its Q-loop region. VHZ was originally classified as an atypical DSP and named after its prototypical member as VH1-related protein member Z. In previous work, we presented results indicating that VHZ should be classified as a PTP rather than a DSP, on the basis of a structural analysis and results of a phosphopeptide substrate screen in which VHZ showed activity against pY–containing peptides but not toward pS- or pT-peptides (8).

In the present work, we show that the catalytic activity of VHZ was significantly underestimated in previous reports, as a result of pronounced product inhibition, and the inhibitory effect of certain buffers. Despite much in common with classical PTPs, VHZ is highly unusual in possessing two acidic residues in the active site, D65 and E134. Our results indicate that under certain circumstances either of these residues can serve as the general acid in the first step of the reaction. We also present results demonstrating that VHZ, despite the presence of a Q-loop, catalyzes phosphoryl transfer to alcohols (alcoholysis) in addition to water (hydrolysis) (Scheme 2).

The mutagenesis of several residues in VHZ in parallel with SsoPTP has revealed that, in addition to the Q-loop, particular residues in the general acid IPD-loop play a crucial role in

nucleophilic selectivity. A combination of kinetics and mutagenesis experiments have revealed unusual aspects of the kinetic behavior of VHZ and given insights into factors that control the phosphotransferase activity of VHZ, and possibly in other PTPs.

Experimental Procedures (Materials and Methods)

Protein cloning, expression and purification

VHZ mutants were made using the Qiagen QuikChange Lightning Site-Directed Mutagenesis Kit. VHZ and mutants were purified as previously described (8). A His-tagged version of VHR was prepared as follows. In the first step the gene of VHR was amplified from pT7-7 plasmid using the following primers: Fwd1: **GAA AAC CTG TAT TTT CAG GGC** ATGTCGGGCT CGTTCGAGCT, Rev1: GGA **GAG CTC** CTA GGG TTT CAA CTT CCC CTC CTT GGC TAG to incorporate TEV protease cleavage site (Fwd1, in bold) immediately upstream of the protein gene, and Sac-I restriction site (Rev1, in bold) was added at the end of the gene sequence. In the second step, the product of the first PCR step was used as a template and a KpnI restriction site was added upstream of the TEV protease cleavage sequence using the following set of primers: Fwd2: CGG**GGTACC**GAAAACCTGTAT, Rev1: GGA **GAG CTC** CTA GGG TTT CAA CTT CCC CTC CTT GGC. The resulting PCR product was digested with Kpn-I and Sac-I (Fermentas) and ligated into the pet-45(B+) vector (Novagen) pre-digested with the same set of restriction enzymes. The *E. coli* DH5α competent cells were transformed with 5 μL of the ligation mixture and plated on an ampicillin-containing agar plate. DNA sequencing confirmed the presence of the desired gene. BL-21 DE-3 (codon+) *E. coli* competent cells were transformed with the peT-45(B+) -VHR vector. 10 mL of LB media were inoculated with a single colony and incubated at 37°C on a shaker overnight. 1L of 2xYT media containing ampicillin and chloramphenicol were inoculated with 10 mL of overnight cell growth. The cells were grown at 37°C until OD_{600nm} reached 1.2–1.5 a.u. 100 mg of IPTG were added (final concentration 100 mg/L), the flask was transferred to a room temperature shaker and incubated for 18–20 hours. The cells were harvested by centrifugation and resuspended in Ni loading buffer containing 50 mM Tris, 500 mM NaCl, 20 mM imidazole, 5 mM 2-mercaptoethanol, 5 % glycerol, pH 8.0. Cells were sonicated on ice, and after centrifugation the supernatant was decanted and filtered through 0.45 micron Millipore syringe filter. Ni-fast flow High Affinity Resin (GE Healthcare) was washed 3 times with Ni loading buffer and incubated with supernatant for 30 min at 4° C with gentle shaking. The resin slurry was transferred to a 15 mL glass chromatography column. The column was extensively washed with Ni loading buffer to reach baseline absorbance and protein was eluted with a 120 mL linear gradient with buffer containing 50 mM Tris, 500 mM NaCl, 20 mM imidazole, 2-mercaptoethanol, 5 % glycerol, pH 8.0 at 2 mL/min. The fusion VHR protein obtained was dialyzed stepwise in TEV-cleavage buffers containing 50 mM Tris-Base, 0.5 mM EDTA, 3 mM DTT, 5% glycerol and reducing concentration of NaCl (300 mM, 150 mM, 0 mM), at 1.5 hour per step followed by addition of 2 mg of TEV protease. The cleavage of VHR was rapid and complete in two hours at 4 ° C. VHR was dialyzed in the original Ni-loading buffer to remove DTT and EDTA for two hours, and the solution was passed through Ni-Fast flow High Affinity Resin to remove cleaved polyhistidine tag and TEV-protease. Collected supernatant was concentrated to 3–5 mL using Millipore Centrifuge Concentrator tube and loaded on Superdex 75 26/60 gel filtration column (GE-Healthcare) pre-equilibrated with buffer containing 50 mM HEPES, 150 mM NaCl, 50 mM Imidazole, 5 mM DTT, 10 % glycerol. A single peak corresponding to the VHR was collected, concentrated to 6 mg/mL, flash-frozen in the liquid nitrogen and stored at −80 °C.

Cloning and purification of SsoPTP

The *S.solfataricus* PTP gene sequence from Uniprot (ID Q97VZ7) was optimized for the *E. coli* expression system and synthesized by GenScript delivered in a shuttle vector. The gene was ordered with a KpnI restriction site followed by TEV cleavage site directly upstream of the SsoPTP sequence and a SacI restriction site directly downstream of the stop codon. The shuttle vector containing the described gene was amplified in *E. coli* DH5α, isolated, and digested with KpnI –SacI restriction enzymes in the Green Buffer (Fermentas). The digestion products were separated by electrophoresis using 1% agarose gel. The band correspondent to the desired gene was extracted using Qiagene Gel Extraction Kit and ligated into pet45 (B+) plasmid pre-digested with the same set of restriction enzymes. Unfortunately, unlike VHR (and similar to VHZ(8)), the resulting fusion protein was resistant to TEV cleavage, so the poly-His tag and TEV-cleavage site was removed from the pet45B(+)-SsoPTP vector by one-step overlapping PCR using the following primers: Fwd: TATACCATGTACTGGGTCCGTCGCAAAACG; Rev: GACCCAGTACATGGTATATCTCCTTCTTAAAGTAAACAAAATTATTCTAG. Tagless SsoPTP was expressed in *E. coli* BL-21 DE-3 (codon+) cells. The growth and expression conditions were analogous to VHZ and VHR. The cells were harvested by centrifugation and resuspended in the buffer containing 50mM Tris, 1mM EDTA, 10 mM DTT, 5% glycerol pH 7.4 (4°C). Cells were disrupted by sonication on ice, and the pellet was separated by centrifugation. The supernatant was treated with a 10 % w/v solution of polyethyleneimine (PEI, Mw 50000, pH 8.0 at 4 °C) added dropwise at 4°C to reach a final PEI concentration of 0.5% (w/v). After centrifugation the supernatant was loaded at 1mL/min on a Q-HiTrap (GE Healthcare) column pre-equilibrated with buffer containing 50 mM sodium acetate, 1 mM EDTA, 3 mM DTT, pH 5.5. After washing the protein was eluted with a 120 mL linear gradient (2 mL/min) buffer containing 50 mM sodium acetate, 1 mM EDTA, 600 mM NaCl, 3 mM DTT, pH 5.5. A single isolated peak eluted at 200–250 mM NaCl corresponding to SsoPTP, concentrated to 3–5 mL and loaded on a Superdex 75 26/60 gel filtration column (GE-Healthcare) pre-equilibrated with buffer containing 25 mM Tris, 50 mM imidazole, 150 mM NaCl, 1 mM EDTA, 5 mM DTT, pH 7.5 (at 4°C). A single peak was collected, concentrated to 10 mg/mL (A_{280} of a 1 mg/mL solution = 2.36) and flash frozen in liquid nitrogen in the same buffer with 25% of glycerol added.

YopH, PTP1B and their mutants were expressed and purified as previously described (10, 11).

All enzymes were purified to 99% + homogeneity based upon SDS PAGE analysis (data not shown). Concentration of each enzyme was determined by measuring absorbance at 280 nm using calculated extinction coefficients.

Preparation of p-nitrophenyl phosphate (pNPP)

The dicyclohexylammonium salt of *p*NPP was synthesized as previously described (12). A phosphate free solution of *p*NPP was prepared in two separate steps. The crude product was dissolved in a minimal volume of 0.8 M NaOH. Neutral cyclohexylamine was extracted with five equal portions of chloroform, accompanied by reduction of pH to 8.0–8.5. Inorganic phosphate was precipitated by addition of a solution containing 1M MgCl and 5 M NH_4Cl (1:5 ratio of Mg^{2+}/NH_4^+) to reach 0.1 M final magnesium concentration. The pH was adjusted to 9.0–9.3 with ammonium hydroxide and stirred for 10 minutes until the solution turned cloudy due to the precipitation of $MgNH_4PO_4$. The concentration of *p*NPP in solution remains essentially unchanged, in contrast to calcium or magnesium chloride precipitation alone, which mostly precipitates *p*NPP. The precipitate was removed by filtration using a fritted glass funnel, and 10 g of pre-activated Chelex100 resin suspension in water (pH 9.0) was added to scavenge the remaining magnesium. The resin was removed

by filtration, and cyclohexylammonium hydrochloride (Fisher) solution (pH 8–9) was added. The dicyclohexylammonium salt of *p*NPP precipitated, collected by filtration, washed with cold absolute ethanol, and dried overnight under vacuum to yield phosphate-free dicyclohexylammonium salt of *p*NPP as a white solid, which was stored at −20 °C under nitrogen.

The sodium salt of *p*NPP allows preparation of stock solutions of higher concentrations, and was produced by dissolving the dicyclohexylammonium salt, obtained above, in 0.8 M NaOH solution followed by removal of cyclohexylamine by chloroform extractions. The pH of the aqueous layer was adjusted to pH 12 with 0.1M NaOH, as necessary. A small amount (0.5–1 g) of Amberlite IR120 H resin, extensively pre-washed with deionized water, was added to the solution and stirred for 1 minute. When pH reached 6.0–6.5 the resin beads were removed by filtration. The solution was adjusted to pH 8.5 with dilute sodium hydroxide, and stirred on ice under reduced pressure overnight to remove any traces of organic solvent. The concentration of the stock solution was assayed by adding 10 uL of the *p*NPP solution to 1 mL of 100mM Tris buffer (pH 10) followed by complete hydrolysis with alkaline phosphatase. The final concentration of liberated *p*-nitrophenol was found using the value of λ_{400}= 18300 $M^{-1}cm^{-1}$.

Quantification of inorganic phosphate

A malachite green assay was used to determine the concentration of inorganic phosphate in the *p*NPP substrate, and the concentration of inorganic phosphate in inhibition studies. Briefly, 1.5 g of ammonium hexamolibdate were dissolved in 85 mL of deionized water. The volume was adjusted to 100 mL with 15 mL of concentrated (60.5%) perchloric acid yielding Solution A. The use of perchloric acid was found to improve sensitivity and rate of the color development. Malachite green hydrochloride (0.2 g) were added to 50 mL of solution A with stirring. After 30 min the dark orange solution was centrifuged to separate any undissolved particles yielding Solution B. Solution A was used to adjust Solution B to a final A_{450} = 15 a.u. (measured by assaying diluted aliquots and calculating back to the original concentrate). In a separate 250 ml Erlenmeyer flask 2.5 g of hydrolyzed PVA (Acros) were stirred in 100 mL of deionized water under gentle heating avoiding boiling for several hours to yield clear colorless Solution C (2.5% w/v). Prior to use 2 ml of solution C were added to 10 mL of adjusted Solution B and mixed to yield a dark brown working solution. In a 96 well plate 280 μL of working solution were mixed with 30 μL of diluted phosphate standards in the 0–200 μM range. The color was fully developed in 3–5 minutes and absorbance measured at 625 nM was plotted versus inorganic phosphate concentration to obtain a calibration curve.

Determination of inhibition constants

The effect of buffers and other inhibitors on the activity of VHZ was tested with *p*NPP (sodium salt) in 50 mM sodium acetate buffer (pH 5.5), which showed no inhibitory effect, with inhibitor concentrations in the range 25–200 mM. The data was fitted to several inhibition models using non-linear least squares fit (Origin 8.5.1) with the competitive model yielding the best results in all cases.

Steady-state kinetic analysis

All reactions were performed in non-inhibitory buffers in the presence of 1mM DTT and constant ionic strength adjusted to 150 mM with NaCl at 25 °C. The following buffers, which showed no inhibition against VHZ, were used: pH 4.75–5.5, sodium acetate; 5.75–6.5, sodium succinate; 6.75–7.25, 3,3-dimethylglutarate. All buffers were 50 mM. At least eight substrate concentrations ranging from 0.5–4 x K_M were used for each enzyme to obtain Michaelis-Menten curves. Reaction progress was followed continuously by the

change in absorbance at 400 nm at each pH using a VersaMax plate reader (Molecular Devices). Partial extinction coefficients obtained as described in the SI were used to convert the measured absorbance values into amount of *p*-nitrophenol released. VHZ was susceptible to product inhibition, so linear initial velocities were used at each substrate concentration. Control reactions in the absence of enzyme verified that non-enzymatic hydrolysis could not be detected during the time spans used for enzyme kinetics. The initial rates were plotted vs. substrate concentrations and fitted to the Michaelis-Menten equation using Origin 8.5.1 to obtain kinetic parameters k_{cat} and K_M. The values of k_{cat} and k_{cat}/K_M were plotted versus pH and fitted to the equations shown in the SI to obtain the pK_a values of catalytically important ionizable residues, presented in the Table S1.

Isotope effect measurements

Kinetic isotope effects (KIEs) on the VHZ-catalyzed reaction with *p*NPP were measured using the competitive method, and thus are isotope effects on *V*/*K*. Figure 2 shows the positions where KIEs were measured in the substrate and the designations used. Natural abundance *p*NPP was used for measurements of $^{15}(V/K)$. The ^{18}O KIEs $^{18}(V/K)_{bridge}$ and $^{18}(V/K)_{nonbridge}$ were measured by the remote label method, using the nitrogen atom in *p*-nitrophenol as a reporter for isotopic fractionation in the labeled oxygen positions (13). The isotopic isomers used are shown in Figure 2, and their synthesis was as previously described (14). KIEs were measured at pH 5.5 using the buffer 100 mM acetate, 1 mM DTT, 0.5 mM EDTA. The reactions were conducted at 25°C and [*p*NPP] = 25 mM. All reactions for bridged, non-bridged and natural abundance isotope effects were performed in triplicate and the progress was monitored continuously by measuring absorbance at 400 nM. Reactions were stopped at 40, 50 and 60 % completion by acidification to pH 3.0 with HCl, which caused some precipitation of protein, which was separated by centrifugation. To remove remaining enzyme, the reaction solution was centrifuged in a Millipore Amicon-Ultra 3kDa protein concentrator. The resulting solution was extracted with three 50 mL portions of diethyl ether. Ether fractions were collected, dried with anhydrous magnesium sulfate, filtered, and ether was removed by rotary evaporation. The unhydrolyzed *p*NPP remaining in the aqueous layer was hydrolyzed using alkaline phosphatase after the pH was adjusted to 10 by addition of 1 M Tris to pH 11. After 8 hours the *p*NP product was extracted and collected as previously described. After sublimation the *p*-nitrophenol samples were analyzed by isotope ratio mass spectrometry. The isotope effect was calculated from the nitrogen isotopic ratios in the *p*-nitrophenol product at partial reaction, in the residual substrate, and the starting material, as described in Supporting Information. The $^{18}(V/K)_{nonbridge}$ values were corrected for the dianionic fraction of *p*NPP at pH 5.5.

Detection of phosphotransferase activity in the presence of ethylene glycol

The hydrolysis of *p*NPP by VHZ and VHZ/P68V was monitored using a JEOL 300 MHz NMR spectrometer at the 121.5 MHz ^{31}P resonance frequency. Reaction was started by addition of VHZ to a solution containing 20 mM *p*NPP in 50 mM sodium acetate (pH 5.5), 0.5 mM EDTA, 3mM DTT and 1M ethylene glycol. The instrument was locked using D_2O in a coaxial tube. The instrument was set to collect 64 scans, relaxation delay 4 sec, sweep 50 ppm.

The dependence of k_{cat} was measured as a function of ethylene glycol concentration for VHR, VHZ, VHZ/E134Q, VHZ/E134A, VHZ/D65A, VHZ/P68V, SsoPTP, and SsoPTP/V72P by monitoring release of *p*-nitrophenol. Reactions were performed in 50 mM sodium acetate buffer (pH 5.5) and concentration of ethylene glycol varied in the range of 0–3 M.

Pre-steady state kinetics

Measurement of *p*NPP hydrolysis catalyzed by VHZ, VHR, as and VHZ/D65A mutant were performed at 25 °C using a stopped-flow spectrophotometer (KinTek). Release of *p*-nitrophenol was monitored by increase in absorbance at 400 nM in 100mM succinate buffer (pH 5.85), using an extinction coefficient corrected for this pH (see SI). Enzyme concentration varied in the range 20–65 μM. The *p*NPP concentration was 20 mM for VHZ/D65A, and 50 mM for VHR/WT and VHZ. Absorbance traces of at least five separate experiments at each substrate and enzyme concentration were averaged. The data was fitted to the equation [p-nitrophenol] = At + B (1-e^{-kt}). At saturating concentrations of substrate, k = $k_3 + k_5$. The linear steady-state phase A = $k_3k_5 / (k_3 + k_5)$. The magnitude of the burst B = $E_o [k_3 / (k_3 + k_5)]^2 / (1 + K_M / S_o)^2$.

Computational analysis of pNPP binding to VHZ

The computational packages AutoDock (15, 16) and FlexX (17) were used to model the docking of *p*NPP in the active site of VHZ. The 1.15 Å resolution crystal structure of the VHZ-metavanadate complex (PDBID: 4ERC) was used as the starting model. The VO_3 ligand at the active site was removed, and the following charges/protonation states were assigned to the residues: C95 (−1); H94 and R101,(+1); D65 and E134, neutral. The side chains of D65, F66, L97 and E134 residues were treated as flexible, the rest of the protein was rigid. The *p*NPP ligand coordinates were extracted from the crystal structure of SsoPTP (PDBID: 2I6P) and the di-anionic form of the phosphate ester was used for docking. Free rotation was allowed around the phosphate monoester bond, while the *p*-nitrophenol ring was treated as planar and rigid. The Lamarckian Genetic algorithm was selected for its reliability and ability to calculate “deeper minima” (18) and the search was conducted within a 15 Å grid region centered at the active site.

Results

Buffer and Oxyanion Inhibition

The effects of buffers and oxyanions on the catalytic activity of VHZ are summarized in Table 1. No inhibitory effects were observed for acetate, succinate, 3,3-dimethylglutarate, or diglycine. VHZ is weakly inhibited by triethanolamine hydrochloride and cyclohexylamonium hydrochloride, while N-ethyl morpholine (NEM) hydrochloride displayed no inhibitory effect. As expected, the sulfonate containing buffer HEPES showed relatively strong inhibition. Cyclohexylammonium is a common counterion for the commercially available substrate *p*NPP, and although its effect was relatively weak, the sodium salt was used in all experiments.

Kinetic Isotope Effects

The KIEs in the positions shown in Figure 2 for the VHZ-catalyzed hydrolysis of *p*NPP are presented in Table 2, together with previously reported KIEs for PTP1B and VHR. The $^{18}(V/K)_{nonbridge}$ KIEs for VHZ are very similar to these precedents (10, 19), suggesting that, like these related enzymes, the VHZ-catalyzed reaction proceeds via a loose transition state. The $^{18}(V/K)_{bridge}$ KIE is higher in VHZ and a significant magnitude for the $^{15}(V/K)$ isotope effect contrasts with the absence of a measureable KIE in this position in the other two phosphatases. Both observations are consistent with incomplete neutralization of the leaving group by the general acid in the transition state.

Steady-state kinetics analysis

Table 3 shows the kinetic parameters, k_{cat}, K_M, and k_{cat}/K_M for VHZ, VHR, YopH, PTP1B, SsoPTP, and several VHZ mutants, measured at pH 5.5 at 23 °C. This corresponds to the pH

optimum of many PTPs, including VHZ. The kinetic parameters for VHR, YopH, and PTP1B measured by continuous assay at 400 nm are in good agreement with the literature values. We obtained values of k_{cat} = 3.9 s^{-1} and K_M = 8.3 mM for *p*NPP hydrolysis by VHZ at the pH optimum of 5.5, compared with previously reported k_{cat} = 0.009 s^{-1} and K_M = 1.5 mM (20). The revised k_{cat} is comparable to those of native VHR and *Sso*PTP. The K_M is significantly higher than previously reported, resulting in lower overall enzymatic efficiency (k_{cat}/K_M).

pH dependency for the hydrolysis of pNPP by VHZ

The pH-rate profiles for native VHZ and the mutants D65A and E134Q are shown in Figure 3. The pK_a values of ionizable residues were determined by non-linear least squares fitting of experimental data to the appropriate equations (see SI), for k_{cat} and k_{cat}/K_M, and shown in Table S-1. The second ionization constant for *p*NPP was set to the literature value of 4.96 (12). The pK_a values obtained are in good agreement with those previously obtained for other PTPs, and the bell-shaped profiles are typical of the PTP family. The acid limb is ascribed to the deprotonated C95 nucleophile, which has an unusually low pK_a due to stabilizing influences of the neighboring H94 in VHZ. The basic limb is ascribed to general acid catalysis in the first step consistent with the PTP mechanism (Scheme 1).

The IPD-loop in VHZ bears the putative D65 general acid. This loop and the position of the acid correspond to the conserved WPD-loop in classical PTPs (Figure 4). D65 was proposed to be the general acid catalyst by structural analogy, and based on the observation of lost hydrolysis of *p*NPP by the D65A mutant (21, 22). In our hands, the D65A mutation resulted in a 5-fold reduction of k_{cat} and a 40-fold reduction of K_M. The pH-rate profile remains bell-shaped (Figure 3). In contrast, the analogous mutation of the general acid in other PTPs to alanine or to asparagine results in a 100 to 1000-fold reduction in k_{cat}, and the loss of the basic limb in the kinetic pH-rate profile, indicating loss of general acid catalysis (23, 24). In contrast, the kinetic constants for the D65N mutant are similar to those of native VHZ (Table 3).

The active site of VHZ possesses another acid (E134 from the Q-loop) in position to potentially protonate the leaving group (Figure 4). The E134Q and E134A mutations both reduced k_{cat} by about an order of magnitude (Table 3) with no significant effect on K_M. The pH profile of the E134Q mutant remained bell-shaped. Only the simultaneous removal of both general acids (D65N/E134Q) led to a significant reduction of k_{cat} and loss of the basic limb of the pH-rate profile (Figure 3). The double mutants precipitated below pH 5.25, precluding measurement of kinetic data below this pH.

Pre-steady state kinetics

Many PTPs, including YopH, PTP1, and VHR, exhibit burst kinetics, indicating that the second step is rate-limiting (3, 25). When native VHR was rapidly mixed with *p*NPP a pre-steady state burst of *p*-nitrophenol release was observed (Figure 5). The values of k_3 and k_5 obtained for VHR are close to those previously reported (25). Under the same conditions native VHZ and its E134Q mutant revealed no pre-steady state burst. In contrast, the VHZ/D65A mutant displayed a pre-steady state burst stoichiometric with the amount of enzyme. Values of k_3, k_5 and K_S (the true substrate binding constant) were calculated for native VHR and VHZ/D65A and are presented in Table 4. Although the decrease in the ratio (k_5/k_3) in VHZ/D65A reduces K_M (see SI), it does not fully explain the magnitude of the reduction, indicating that K_S is reduced as well. Despite the absence of a burst, the value of K_S for native VHZ can be calculated if we assume that the primary role of D65 is orienting the nucleophilic water in the second step. This assumption is supported by the negligible effect on k_{cat} of the D65N substitution. By setting k_3 for native VHZ equal to that of D65A, the

other elementary rate constants for the reaction of the native enzyme were calculated as shown in Table 4. The VHZ/D65A substitution decreases the magnitude of K_S 14-fold. Because substitution of D65 with A (but not N) increases enzyme substrate affinity, we conclude the existence of an unfavorable steric, rather than electrostatic, interaction between D65 and the aromatic ring of the substrate. The K_i for inorganic phosphate is lower than K_S for *p*NPP in both native VHZ and VHZ/D65A. However, whereas K_S for *p*NPP is reduced 14-fold by the removal of D65 side chain (Table 4), the K_i for inorganic phosphate is reduced only ~ 1.5-fold (Table 1).

Reaction in the presence of ethylene glycol—The dependence of k_{cat} on ethylene glycol concentration was measured for native VHZ and several mutants. It should be noted (discussed in the SI) that the slope of such a plot where $k_{cat} = k_5 + k_7 \times[ROH]$ yields the second order rate constant for ethylene glycol phosphorylation (k_7, Scheme 2) only when $k_3 >> k_5$. In the more general case, when no distinct rate-limiting step exists and no pre-steady state burst is present, the expression $k_{\mathrm{cat}}=\frac{k_3 \times k_5}{k_5+k_3}+\frac{k_3 \times k_7}{k_5+k_3} \times [\mathrm{ROH}]$ holds and interpretation of the calculated slope is more complex. However, the nucleophilic *Slope* selectivity $S=\frac{Slope}{Intercept}=\frac{\frac{k_3\times k_7}{k_5+k_3}}{\frac{k_3\times k_5}{k_5+k_3}}=\frac{k_7}{k_5}$ (Table 5, column 3) is independent of k_3 and reflects the relative preference for alcoholysis over hydrolysis.

The E134Q mutation results in no significant change in phosphotransferase ability. The E134A mutation significantly increases the alcoholysis to hydrolysis ratio, indicating that E134 participates in the second step of the reaction, like Q446 in YopH. Although Q-loop residues in PTPs are generally thought to control access to the phosphoenzyme intermediate, the D65A mutation on the IPD-loop has a more pronounced effect than E134A. Because the closely related SsoPTP lacks phosphotransferase activity, we compared the effects of mutations on the IPD-loops in VHZ and SsoPTP. The SsoPTP contains only two proline residues on its IPD-loop, P68 and P73, corresponding to P64 and P69 in VHZ. These residues are highly conserved in classical PTPs (see the sequence alignment in Figure 8) and mutations result in similar, adverse catalytic effects in VHZ (Table 3). VHZ possesses another proline, P68, which is occupied by V72 in SsoPTP. The VHZ/P68V mutation abolished phosphotransferase activity (Figure 6). This effect was further supported by ^{31}P NMR spectroscopy shown in Figure 7. The orthogonal SsoPTP/V72P mutation conferred phosphotransferase ability comparable to that of native VHZ.

Discussion

Although VHZ is related to classical PTPs and utilizes the same mechanism (8) it differs in several important ways from most PTP family members.

VHZ is inhibited by commonly used buffers, and by inorganic phosphate more strongly, than typical PTPs

Previous kinetic investigations of VHZ utilized single time point assays after 20 or 30 minutes, and buffers containing Tris (20, 22) or Bis-Tris, which are weak competitive inhibitors (Table 1). Although the inhibition constants are in the high millimolar range, buffers are typically used at such concentrations. While buffers containing the sulfonate functional group, such as HEPES, are recognized as inhibitors of PTPs, and have been observed in some PTP crystal structures, the inhibition of VHZ by buffers such as Tris and triethanolamine was unexpected. This behavior may result from the combined effect of several anionic residues near the VHZ active site (D65, E44, E134 and E137) but the molecular origin of buffer inhibition was not tested. The inhibition constant for inorganic

phosphate is lower than in classical PTPs, and is significantly lower than the K_S for *p*NPP (Table 4). Probable structural origins for this difference are discussed below. The net effect of these properties led to a significant underestimation of VHZ activity in previous reports.

In addition to avoiding inhibitory buffers, we validated a method for the continuous collection of rate data using the substrate *p*NPP monitoring reaction progress at 400 nm using extinction coefficients measured at the experimental conditions (see SI). Continuous monitoring of the reaction showed that VHZ becomes inhibited by product after several minutes. Finally, commercial *p*NPP, which often contains small but experimentally significant amounts of inorganic phosphate, was used in previous studies. We developed a purification strategy to minimize contamination by inorganic phosphate, that also offers a simple means to convert the di-cyclohexylammonium salt to the more soluble disodium salt.

Using non-inhibitory buffers, a continuous assay, and phosphate-free substrate, VHZ proved to be significantly more active than previously reported (k_{cat} = 3.9 s^{-1} versus 0.009 s^{-1}). We also developed a process for the expression and purification of the native enzyme with no tags. Although previous reports used tagged versions of VHZ, the difference in activity is too significant to be explained by the absence of tags. Furthermore, discontinuous assays of tagless VHZ using the previously reported methods yielded results similar to the previous reports (20, 22).

The leaving group is not fully neutralized in the first step of the VHZ reaction

The KIEs for the hydrolysis of *p*NPP have been reported for a number of PTPs including YopH (26), PTP1B (27), VHR(19), and the LMW PTP Stp1(28). Because these are measured by the competitive method, the KIEs reflect the portion of the kinetic mechanism up to the first irreversible step, cleavage of *p*NPP. The mechanistic origins of the KIEs for *p*NPP hydrolysis have been described elsewhere (13). In brief, a normal $^{15}(V/K)$ up to a maximum of 1.003 arises from negative charge development on the leaving group. Efficient general acid catalysis by PTPs abolishes this effect, resulting in a $^{15}(V/K)$ of unity. Fission of the P-O bond produces a normal $^{18}(V/K)_{bridge}$ effect. Simultaneous leaving group protonation produces an inverse effect that partially reduces the normal effect from P-O cleavage. Thus, in general acid mutants, $^{18}(V/K)_{bridge}$ is typically ~ 1.03, compared to ~1.015 in native PTPs. The $^{18}(V/K)_{nonbridge}$ KIE responds to change of hybridization state of the phosphoryl group. This KIE is slightly inverse to near unity in PTPs, reflecting the loose metaphosphate-like transition state; associative transition states result in normal values.

Both of the oxygen isotope effects for the VHZ reaction are within experimental error of previous data with PTP1B and VHR (Table 4). In contrast, the $^{15}(V/K)$ differs from the other PTPs and is slightly normal, indicating that the leaving group is not completely neutralized in the transition state. The magnitude suggests approximately 1/3 of a negative charge, from protonation that is not fully synchronous with P-O bond fission. This has been observed in one previous PTP family member, the LMW PTP Stp1(28). Incomplete protonation of the leaving group in the first step may contribute to a reduction of k_3 and explain the absence of a burst in the VHZ catalyzed reaction of *p*NPP.

Two potential and functional general acids in the active site of VHZ

The D65 residue resides on the IPD-loop, a structure analogous to the WPD-loop in classical PTPs that bears the conserved general acid (Figure 8). The E134 residue in VHZ is superimposable with a conserved Q residue located on the Q-loop in classical PTPs that orients the nucleophilic water in the second step (29). The pH rate profiles of the D65 and E134 mutants both retain their basic limbs. The D65N mutation has no significant effect on

catalysis, and the D65A and E134Q mutations have k_{cat} values that are reduced by only an order of magnitude. Only in the double mutant is catalysis reduced to the extent seen in general acid mutants of other PTPs, consistent with complete elimination of general acid catalysis. We conclude the D65 and E134 single mutants both retain general acid function. We conclude that native VHZ utilizes E134 as the primary general acid, with a minor contribution from D65, which becomes the major general acid when E134 is mutated. The data suggest that, unlike any other known PTP or DSP, VHZ contains two acidic residues in the active site, either of which can protonate the leaving group in the absence of the other.

One might consider whether these results arise from the good leaving group in *p*NPP that may not need an enzymatic general acid to protonate it at the acidic pH optimum. However, several lines of evidence show that general acid catalysis is part of the mechanism of *p*NPP hydrolysis by PTPs, and with other substrates. KIE results at the acidic pH optima across the PTP family show that the leaving group leaves as the neutral phenol in native enzymes, but is charged when the enzymatic general acid is mutated. In such mutants the rates of *p*NPP hydrolysis are significantly reduced, and pH-rate profiles lose their basic limbs (13).

D65 has a role primarily in the second step, and affects substrate binding— The fact that the D65N mutation does not significantly affect activity, while the D65A mutation does, suggests that the reduced catalysis in the D65A mutant arises due to inability of the alanine side chain to participate in phosphoenzyme hydrolysis by orientation of the nucleophilic water. In this sense, the roles of D65 and E134 are reversed from classical PTPs, in which the conserved glutamine corresponding to E134 positions the nucleophilic water, and the acid corresponding to D65 is the general acid in the first step and a general base in the second step.

The D65A mutation significantly reduces K_M and K_S. This effect is less pronounced for mutations of the corresponding residue in other PTPs. This may be explained by fact that in classical PTPs this residue resides on the mobile WPD-loop, which is primarily in an open conformation in the free enzyme. Because the IPD-loop in VHZ is permanently closed (8), the D65 side chain is fixed in a position that restricts access to the deep and narrow VHZ active site. DSPs, such as VHR, also have a non-movable general acid loop; however, in these enzymes the general acid is positioned on another side of the active site (Figure 4), and presents less steric hindrance to incoming ligands. This explains the higher K_M for *p*NPP in VHZ compared to other PTPs. The structurally analogous SsoPTP, which also contains a rigid IPD-loop, has a K_M value approximately 3-fold lower than VHZ and comparable to that of VHR. However, unlike VHZ, which has a narrow and deep active site pocket (8) the active site of SsoPTP is broad and shallow due to the presence of multiple surrounding glycine residues in the P-loop and IPD-loop (Figure 8).

Neither D65A nor D65N substitution significantly affects the K_i for inorganic phosphate (Table 1). It also confirms that the mutation of D65 side chain side chain does not disrupt the P-loop, which serves as the dominant binding element to the anionic phosphoryl group. In contrast, the D65A mutation lowers the Ks for *p*NPP 14-fold. This suggests the effect of D65 substitutions on binding is primarily steric rather than electrostatic, involving the ester group of the substrate more than the phosphoryl group. This would permit the biological activity of VHZ to be more regulated by levels of intracellular phosphate than most classical PTPs. The intracellular regulation of phosphatases by phosphate has been recently discussed (30). Unlike classical PTPs with much higher K_i values, VHZ, SsoPTP, and VHR have inhibition constants similar to the average physiological concentration of inorganic phosphate (1–1.3 mM) (31).

VHZ has a low catalytic efficiency and different rate-limiting step compared to most PTPs—Despite the fact that VHZ is more active than previously thought, it remains one of the least active PTPs. A significant part of its reduced catalytic efficiency arises from its high K_S. Indeed, for the PTP catalyzed reaction (Scheme 1) $\frac{k_{cat}}{K_M}=\frac{k_3}{K_S}$ (see SI for derivation), which means that VHZ requires a 5–8 fold higher substrate concentration to achieve its limiting velocity. In addition to high K_s values, the k_{cat} for VHZ is lower than classical PTPs. Our data suggest that both steps of the VHZ catalyzed reaction are slower than in classical PTPs, and both contribute to the overall rate ($k_{cat}=\frac{k_5 \times k_3}{k_3+k_5}$) under steady state conditions. According to the KIE results the neutralization of the leaving group in the first step is incomplete, which reduces k_3, but cannot explain the reduction of k_5. It was previously shown that mutations of Q-loop residues in classical PTPs reduces k_5 by 2 orders of magnitude, an effect that was used to trap the phosphoenzyme intermediate of PTP1B (24, 29). The E134Q mutation makes VHZ structurally more similar to classical PTPs and affects only the first step, resulting in the 8-fold reduction of activity. The k_{cat} value of the E134A mutant is 70% that of the E134Q mutant. Such an insignificant reduction from complete removal of the functional group indicates that the residue does not function in the second step like the Q in this position in classical PTPs, explaining the lower k_5 in VHZ compared to other PTPs. The k_5 value of native VHZ is more similar that of VHR (Table 4) which, in place of the Q-loop, (Figure 4) has an N-loop region (Figure 8) that is highly conserved among atypical DSPs.

VHZ has two substrate binding modes for pNPP—The expressions for k_{cat} and K_M for the PTP-catalyzed reaction (Scheme 1), $k_{cat}=\frac{k_5 \times k_3}{k_3+k_5}$ and $K_M=K_S \times \frac{k_5}{k_3+k_5}$ contain the same elementary constants, and thus, any change in k_{cat} is reflected in K_M and vice versa. A reduction in k_3 results in increased K_M as is seen in the VHZ/E134Q/D65N double mutant, in which both general acids important in k_3 are mutated, but k_5 remains unaffected. As k_3 becomes smaller with respect to k_5, K_M approaches K_S. Because of this, the K_M for the VHZ/D65N/E134Q double mutant (Table 3) is close to the K_S for native VHZ determined from pre-steady state kinetics (Table 4). The same effect has been previously observed in the general acid D92N mutant of VHR (23). In contrast, mutations of Q loop residues that do not affect k_3 but decrease k_5, have the opposite effect on K_M. The same trend was previously observed in the Q556M Q446A mutants of YopH (6). The reduction of k_5 reduces the rate of formation of the free enzyme form E, which lowers the K_M parameter in the steady-state experiment. This mutual dependence of k_{cat} and K_M becomes less obvious when $k_3 >> k_5$ but, because in native VHZ the two constants are relatively similar, (consistent with the absence of a burst) even small changes should be easily detected. The E134Q mutation in VHZ eliminates the major general acid but results in only a 10-fold reduction of k_{cat} and has no effect on K_M. The D65N substitution results in a modest rate reduction, consistent with its role as the minor general acid, but also has no significant effect on K_M. The pH rate profiles of both mutants remain bell-shaped, indicating that when one general acid is eliminated, the other one takes over, maintaining general acid catalysis. The kinetic behavior of the mutants suggests the presence of two catalytically equivalent, but differently populated, forms of the Michaelis complex. Similar to the mode of action of a noncompetitive inhibitor on the native enzyme, the E134Q or D65N mutation renders one of the two conformations catalytically unproductive, which reduces the rate but has no effect on K_M.

In order to obtain insights into substrate binding modes in VHZ that might explain how either D65 or E134 can act as a general acid, the programs AutoDock (15, 16, 32, 33) and

FlexX (17) were used to predict the orientation of *p*NPP in the active site. Both programs predicted two possible conformations, presented in Figure 9. In each, the phosphate moiety of the substrate is coordinated by the P- loop and the side chain of R101, and is properly positioned for nucleophilic attack by the negatively charged cysteine at the bottom of the active site. In conformation A the scissile oxygen is oriented towards E134, consistent with its assignment as the primary general acid. The D65 side chain turns away to avoid a steric clash with the *p*-nitrophenyl ring. We conclude that this substrate conformation is the predominant one, consistent with the kinetic effects of the E134Q mutation and steric relief observed in the D65A mutant. The substrate conformation in panel 9B is the one commonly observed in classical PTPs, except for the position of the glutamine residue analogous to E134, which occupies a different conformation to avoid a steric clash with the substrate phenyl ring (29). However, it resembles the position of the corresponding Q135 residue in several structures of SsoPTP in complex with peptide substrates (9). In this conformation the phenolate ring is in close proximity to the L97 side chain, and D65 is oriented in position to donate its proton to the scissile oxygen of the leaving group. This substrate orientation is consistent with the kinetic behavior of the E134Q mutant, which utilizes D65 as its general acid.

The presence of two binding conformations explains why the E134Q and D65N mutants have a reduced k_{cat} with no significant effect on K_M. If conformation B, in which the E134Q mutant can utilize the D65 general acid, presents a minor fraction of the overall enzyme-substrate complex, then it would kinetically appear as a reduction of k_{cat} because the predominant conformation A would be catalytically unproductive in this mutant. The different effects of the D65N and E134Q mutations on k_{cat} with no significant effect on K_M suggest that while both conformations A and B coexist, conformation A dominates. The E134Q or D65N substitution, which results in conformation A or B becoming non-productive, respectively, is similar to the effect from noncompetitive inhibition. Noncompetitive inhibition results from the formation of a non-productive enzyme-substrate-inhibitor complex that reduces V_{max} but has no effect on K_M. The reaction catalyzed by the E134Q mutant where conformation A is unproductive and conformation B leads to product formation according to the equation: $V^{A}_{\max}=\frac{V^{WT}_{\max}}{\left(1+\frac{1}{K_{AB}}\right)}$, where V^{WT}_{max} is the maximal rate of the reaction by the native VHZ, and V^{A}_{max} is the maximal velocity for the E134Q mutant. The calculated value of $K_{AB}=\frac{[B]}{[A]}=0.12$ indicates that about 89% of the VHZ [ES] complex exists in conformation A, and 11% in form B. This ratio is consistent with the modest reduction of k_{cat} in the D65N mutant. The equilibrium constant of 0.12 implies a modest energetic difference of slightly more than 1 kcal/mol, consistent with the nearly equal scoring function obtained from the docking programs for the two conformations.

The predominance of conformation A in which the phenolate ring interacts with the D65 side chain explains the steric relief produced by the D65A mutation. The presence of the E134 general acid and its use in conformation A may be a reasonable evolutionary solution to permit a bulky substrate to enter the narrow and sterically demanding active site pocket. Conformation B is the one the most commonly observed in the classical PTPs, which possess a movable WPD-loop. This conformation allows VHZ to utilize its D65 general acid. However, under the condition of a non-movable general acid-bearing loop, conformation B is sterically disfavored, making it less populated than conformation A. The presence of the two coexisting but unequally populated conformations explains why both the E134Q and D65N mutants retain their basic limbs in the pH-rate profile, but produce proportionally different effect on k_{cat} without affecting K_M.

A similar phenomenon may explain anomalous behavior reported in the Tk-PTP, a protein tyrosine phosphatase isolated from the *Thermococcus kodakaraensis* KOD1. On the basis of structural comparisons with known PTPs, D63 was assigned as the putative general acid. Unexpectedly, the D63A mutant was found to be more active, not less, than the native enzyme (34). No structure of Tk-PTP has been published; however, the protein sequence (Figure S-2) suggests the presence of a glutamic acid residue in a position corresponding to that of E134 in VHZ. Like VHZ, Tk-PTP may utilize a different general acid than the one implicated by structural comparisons with the PTP family.

The finding of two alternate binding modes and two general acids may be physiologically relevant, but the results presented here do not address whether the same flexibility pertains to peptide substrates. Physiological substrates for VHZ have not been confirmed. Recently, the existence of two alternate peptide substrate binding modes, depending on sequence, has been reported for the related enzyme VHR (35). In that case, only a single general acid is in the active site and is used in both conformations.

VHZ exhibits phosphotransferase activity controlled by a single residue in an unexpected location—In classical PTPs, Q-loop residues such as Q446 and Q450 in YopH (Figure 4), in locations analogous to E134 and Q138 in VHZ, position the nucleophilic water for the second step and shield the phosphoenzyme from larger nucleophiles (6). In classical PTPs catalysis is unaffected by added ethylene glycol. In contrast, YopH mutants in which these glutamines are mutated show significant phosphoryl transfer to ethylene glycol (6). This has provided a rationalization for why the native VHR and LMW-Ltp1, which lack an analogous Q-loop, display phosphotransferase activity (7). Thus, the observation of phosphotransferase activity by VHZ was unexpected, since its E134 and Q138 residues are superimposable with Q446 and Q450 in YopH. The ratio S of the second-order rate constant for alcoholysis by ethylene glycol (k_t) to the hydrolysis of the phosphoenzyme intermediate (k_{cat}') is 14.4 (Table 5). This ratio was not significantly affected by the E134Q mutation, indicating that the E and Q residues, as was previously shown with YopH, are interchangeable (6). The higher transphosphorylation by the E134A mutant indicates that that E134 provides some shielding of the phosphoenzyme. However, the analogous YopH/Q446A mutation results in a greater increase, from which we conclude that E134 in VHZ does not function as effectively in the second step as Q446 in YopH. The VHZ/D65A substitution results in the most pronounced increase in the S ratio, which, together with the reduced k_{cat}, indicates that D65 is important in the second step.

Interestingly, unlike VHZ, there is no effect of ethylene glycol concentration on catalysis by SsoPTP. A sequence alignment of the IPD-loops of VHZ and SsoPTP revealed that while SsoPTP contains two proline residues in this region, a pattern that is highly conserved in the PTP family, VHZ has a third proline, P68. In SsoPTP, V72 is found in the corresponding position. The VHZ/P68V mutation results in no significant change in k_{cat}; however, phosphotransferase activity is lost and there is no dependence of rate on ethylene glycol concentration. The orthogonal SsoPTP/V72P mutation confers phosphotransferase ability similar to that of native VHZ. We thus conclude that the single point mutation of proline at the P68 position in VHZ, and the analogous V72 position in SsoPTP, controls the ability of these enzymes to phosphorylate alcohols. Because the IPD-loops in VHZ and SsoPTP are not mobile this mutation has no effect on k_{cat}. Further studies, including structural comparisons, are underway to seek an explanation of how this residue controls phosphotransferase activity.

Conclusions

Although VHZ is more closely related to classical PTPs than to DSPs, it is unique and has a number of unusual properties. VHZ has two functional general acids, and, for the small molecule substrate *p*NPP, two substrate binding modes. Both binding modes are catalytically equivalent but unequally populated. Each binding mode utilizes a different general acid.

Despite the fact that VHZ shares many active site characteristics of classical PTPs, it is a significantly less efficient catalyst. Both catalytic steps k_3 and k_5 are slower. The reduced k_3 is consistent with incomplete neutralization of the leaving group revealed by KIEs. Reduction of k_5 is due to the less efficient involvement of the E134 residue in the second step, as revealed by the E134Q and E134A mutations.

The results also provide a rationale for the advantage of mobility of the general acid-bearing WPD-loop in classical PTPs. The availability of an uncatalytic, open conformation allows the general acid to avoid sterically unfavorable interactions with substrate binding, and to alleviate product release and reduce product inhibition.

The discovery of phosphotransferase activity by VHZ also leads to several conclusions:

1. The fact that the reaction rate increases linearly with ethylene glycol concentration indicates the second step is at least partially rate limiting. Together with the absence of a burst in the pre-steady state, we conclude that both steps contribute to the overall rate.
2. The Q-loop does not fully participate in protecting the active site from incoming alcohol nucleophiles. Mutations in the IPD-loop of VHZ have more effect on phosphotransferase ability. It is logical to conclude that the phosphotransferase activity observed in VH1-related DSPs and Low-molecular weight PTPs can no longer be explained solely by their absence of a Q-loop. The significant difference in position of the general acid loop between classical PTPs, LMW-PTPs and VH1-related DSPs undoubtedly contributes as well.
3. The presence of phosphotransferase activity in some phosphatases, but not others, may have biological consequences. It may not be coincidental that some proteins known to be associated with cancer, such as VH1-related DSPs and LMW-PTPs, and, recently, VHZ(36), reveal a high level of phosphotransferase ability. Whether this process is random and nonspecific, or transphosphorylation is selective for some protein target, remains to be discovered. However, because VHZ has a stringent phosphotyrosine specificity because of its deep and narrow active site, we can conclude that its transphosphorylation target would likely be limited to tyrosine protein sites, or to small molecule nucleophile acceptors capable of entering the active site.

Supplementary Material

Refer to Web version on PubMed Central for supplementary material.

Acknowledgments

We thank Dr. Edwin Antony for use of his stopped-flow spectrophotometer.

This work was supported by National Institutes of Health Grant GM47297 (A.C.H.).

ABBREVIATIONS

KIE	kinetic isotope effect
VHR	Vaccinia H1 related protein member R
LDP	low molecular mass dual specificity phosphatase
VHZ	Vaccinia H1 related protein member Z
***Yop*H**	*Yersinia* outer protein type H
***Sso*PTP**	*Sulfolobus solfataricus* protein tyrosine phosphatase
DSP	dual specificity phosphatase
***p*NPP**	*para*-nitrophenyl phosphate
IPTG	isopropyl β-D-1-thiogalactopyranoside
TEV	tobacco etch virus

References

1. Tonks NK. Protein tyrosine phosphatases: from genes, to function, to disease, *Nature reviews* . Molecular cell biology. 2006; 7:833–846. [PubMed: 17057753]
2. Zhang ZY, Wang Y, Dixon JE. Dissecting the catalytic mechanism of protein-tyrosine phosphatases. Proceedings of the National Academy of Sciences of the United States of America. 1994; 91:1624–1627. [PubMed: 8127855]
3. Zhang ZY, Malachowski WP, Van Etten RL, Dixon JE. Nature of the rate-determining steps of the reaction catalyzed by the Yersinia protein-tyrosine phosphatase. The Journal of biological chemistry. 1994; 269:8140–8145. [PubMed: 8132539]
4. Wang WQ, Sun JP, Zhang ZY. An overview of the protein tyrosine phosphatase superfamily. Current topics in medicinal chemistry. 2003; 3:739–748. [PubMed: 12678841]
5. Patterson KI, Brummer T, O'Brien PM, Daly RJ. Dual-specificity phosphatases: critical regulators with diverse cellular targets. The Biochemical journal. 2009; 418:475–489. [PubMed: 19228121]
6. Zhao Y, Wu L, Noh SJ, Guan KL, Zhang ZY. Altering the nucleophile specificity of a protein-tyrosine phosphatase-catalyzed reaction. Probing the function of the invariant glutamine residues. The Journal of biological chemistry. 1998; 273:5484–5492. [PubMed: 9488671]
7. Paoli P, Modesti A, Magherini F, Gamberi T, Caselli A, Manao G, Raugei G, Camici G, Ramponi G. Site-directed mutagenesis of two aromatic residues lining the active site pocket of the yeast Ltp1. Biochim Biophys Acta. 2007; 1770:753–762. [PubMed: 17296269]
8. Kuznetsov VI, Hengge AC, Johnson SJ. New Aspects of the Phosphatase VHZ Revealed by a High-Resolution Structure with Vanadate and Substrate Screening. Biochemistry. 2012; 51:9869–9879. [PubMed: 23145819]
9. Chu HM, Wang AH. Enzyme-substrate interactions revealed by the crystal structures of the archaeal Sulfolobus PTP-fold phosphatase and its phosphopeptide complexes. Proteins. 2007; 66:996–1003. [PubMed: 17173287]
10. Brandão TAS, Hengge AC, Johnson SJ. Insights into the Reaction of Protein-tyrosine Phosphatase 1B. J Biol Chem. 2010; 285:15874–15883. [PubMed: 20236928]
11. Brandao TA, Robinson H, Johnson SJ, Hengge AC. Impaired acid catalysis by mutation of a protein loop hinge residue in a YopH mutant revealed by crystal structures. J Am Chem Soc. 2009; 131:778–786. [PubMed: 19140798]
12. Bourne N, Williams A. Effective charge on oxygen in phosphoryl group transfer from an oxygen donor. J.Org.Chem. 1984; 49:1200–1204.
13. Hengge AC. Isotope effects in the study of phosphoryl and sulfuryl transfer reactions. Acc Chem Res. 2002; 35:105–112. [PubMed: 11851388]

14. Hengge AC, Cleland WW. Direct measurement of transition-state bond cleavage in hydrolysis of phosphate esters of p-nitrophenol. J. Am. Chem. Soc. 1990; 112(20):7421–7422.
15. Trott O, Olson AJ. AutoDock Vina: improving the speed and accuracy of docking with a new scoring function, efficient optimization, and multithreading. J Comput Chem. 2010; 31:455–461. [PubMed: 19499576]
16. Seeliger D, de Groot BL. Ligand docking and binding site analysis with PyMOL and Autodock/Vina. J Comput Aided Mol Des. 2010; 24:417–422. [PubMed: 20401516]
17. Rarey M, Kramer B, Lengauer T. Time-efficient docking of flexible ligands into active sites of proteins. Proceedings / … International Conference on Intelligent Systems for Molecular Biology; ISMB. International Conference on Intelligent Systems for Molecular Biology. 1995; 3:300–308.
18. Fuhrmann J, Rurainski A, Lenhof HP, Neumann D. A new Lamarckian genetic algorithm for flexible ligand-receptor docking. J Comput Chem. 2010; 31:1911–1918. [PubMed: 20082382]
19. Hengge AC, Denu JM, Dixon JE. Transition-state structures for the native dual-specific phosphatase VHR and D92N and S131A mutants. Contributions to the driving force for catalysis. Biochemistry. 1996; 35:7084–7092. [PubMed: 8679534]
20. Alonso A, Burkhalter S, Sasin J, Tautz L, Bogetz J, Huynh H, Bremer MC, Holsinger LJ, Godzik A, Mustelin T. The minimal essential core of a cysteine-based protein-tyrosine phosphatase revealed by a novel 16-kDa VH1-like phosphatase, VHZ. The Journal of biological chemistry. 2004; 279:35768–35774. [PubMed: 15201283]
21. Takagaki K, Satoh T, Tanuma N, Masuda K, Takekawa M, Shima H, Kikuchi K. Characterization of a novel low-molecular-mass dual-specificity phosphatase-3 (LDP-3) that enhances activation of JNK and p38. The Biochemical journal. 2004; 383:447–455. [PubMed: 15281913]
22. Wu Q, Li Y, Gu S, Li N, Zheng D, Li D, Zheng Z, Ji C, Xie Y, Mao Y. Molecular cloning and characterization of a novel dual-specificity phosphatase 23 gene from human fetal brain. Int J Biochem Cell Biol. 2004; 36:1542–1553. [PubMed: 15147733]
23. Denu JM, Lohse DL, Vijayalakshmi J, Saper MA, Dixon JE. Visualization of intermediate and transition-state structures in protein-tyrosine phosphatase catalysis. Proceedings of the National Academy of Sciences of the United States of America. 1996; 93:2493–2498. [PubMed: 8637902]
24. Flint AJ, Tiganis T, Barford D, Tonks NK. Development of ‘‘substrate-trapping’’ mutants to identify physiological substrates of protein tyrosine phosphatases. Proc. Natl. Acad. Sci. 1997; 94:1680–1685. [PubMed: 9050838]
25. Zhang ZY, Wu L, Chen L. Transition state and rate-limiting step of the reaction catalyzed by the human dual-specificity phosphatase, VHR. Biochemistry. 1995; 34:16088–16096. [PubMed: 8519766]
26. Hengge AC, Sowa GA, Wu L, Zhang ZY. Nature of the transition state of the protein-tyrosine phosphatase-catalyzed reaction. Biochemistry. 1995; 34:13982–13987. [PubMed: 7577995]
27. Brandao TA, Johnson SJ, Hengge AC. The molecular details of WPD-loop movement differ in the protein-tyrosine phosphatases YopH and PTP1B. Arch Biochem Biophys. 2012; 525:53–59. [PubMed: 22698963]
28. Hengge AC, Zhao Y, Wu L, Zhang ZY. Examination of the transition state of the low-molecular mass small tyrosine phosphatase 1. Comparisons with other protein phosphatases. Biochemistry. 1997; 36:7928–7936. [PubMed: 9201938]
29. Pannifer AD, Flint AJ, Tonks NK, Barford D. Visualization of the cysteinyl-phosphate intermediate of a protein-tyrosine phosphatase by x-ray crystallography. The Journal of biological chemistry. 1998; 273:10454–10462. [PubMed: 9553104]
30. Dick CF, Dos-Santos ALA, Meyer-Fernandes JR. Inorganic Phosphate as an Important Regulator of Phosphatases. Enzyme Research. 2011; 2011:1–7.
31. Marshall, WJ.; Bangert, SK. Clinical Biochemistry: Metabolic and Clinical Aspects. Elsevier; 2008. p. 2e
32. Chang MW, Ayeni C, Breuer S, Torbett BE. Virtual screening for HIV protease inhibitors: a comparison of AutoDock 4 and Vina. PLoS One. 2010; 5:e11955. [PubMed: 20694138]
33. Sousa SF, Fernandes PA, Ramos MJ. Protein-ligand docking: current status and future challenges. Proteins. 2006; 65:15–26. [PubMed: 16862531]

34. Jeon SJ, Fujiwara S, Takagi M, Tanaka T, Imanaka T. Tk-PTP, protein tyrosine/serine phosphatase from hyperthermophilic archaeon Thermococcus kodakaraensis KOD1: enzymatic characteristics and identification of its substrate proteins. Biochemical and biophysical research communications. 2002; 295:508–514. [PubMed: 12150979]

35. Luechapanichkul R, Chen X, Taha HA, Vyas S, Guan X, Freitas MA, Hadad CM, Pei D. Specificity profiling of dual specificity phosphatase vaccinia VH1-related (VHR) reveals two distinct substrate binding modes. The Journal of biological chemistry. 2013; 288:6498–6510. [PubMed: 23322772]

36. Tang JP, Tan CP, Li J, Siddique MM, Guo K, Chan SW, Park JE, Tay WN, Huang ZY, Li WC, Chen J, Zeng Q. VHZ is a novel centrosomal phosphatase associated with cell growth and human primary cancers. Mol Cancer. 2010; 128

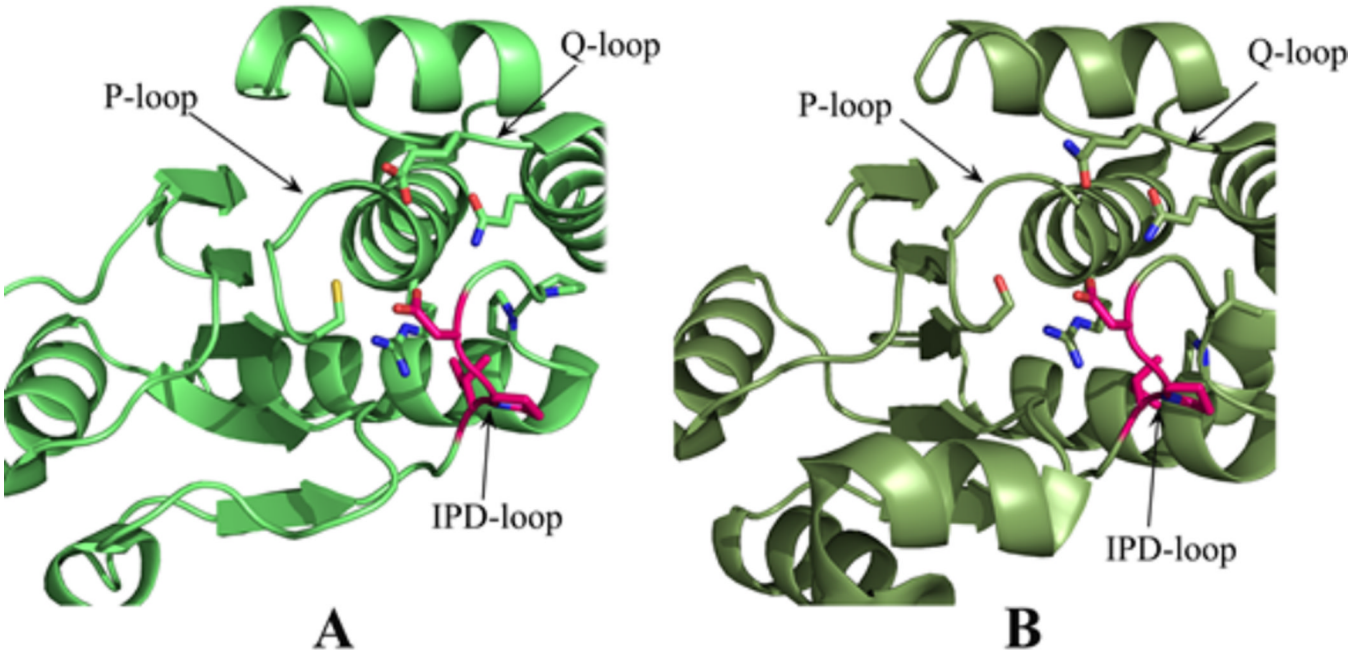

Figure 1.
Side by side comparison of (A) VHZ/PTP (PDB ID 4ERC), and (B), SsoPTP (PDB ID 2I6J). The proteins are very similar in size and structure, and both contain a rigid IPD-loop (highlighted in red) in contrast to the conserved WPD-loop in classical PTPs. Both proteins lack an N-terminal substrate recognition loop and contain no additional extracatalytic domains.

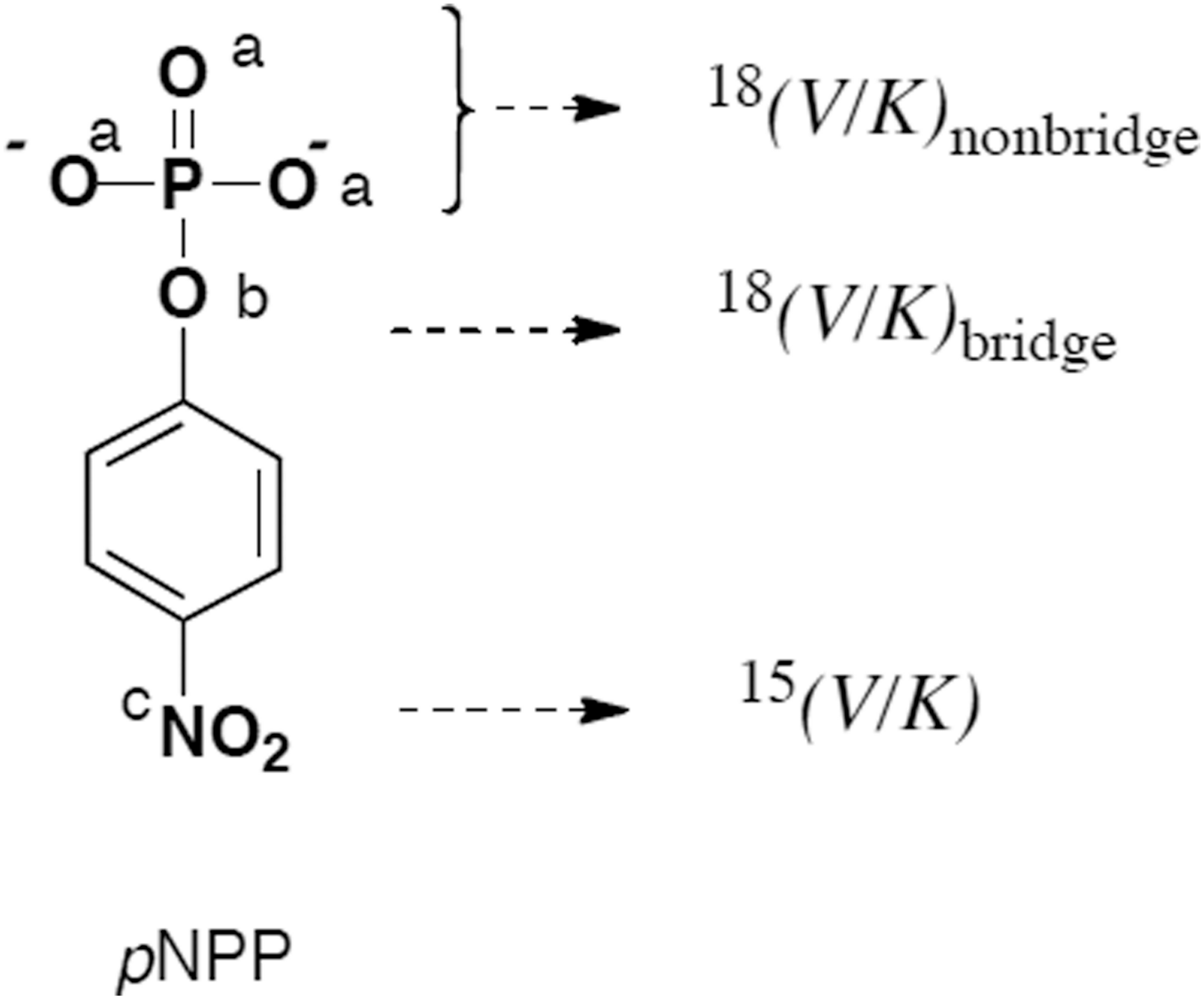

Figure 2.
Positions of KIE measurement in the substrate *p*NPP. Oxygen-18 KIEs were measured at the nonbridging oxygen atoms of the phosphoryl group (a) and the bridging ester oxygen atom (b). The Nitrogen-15 KIE was measured in the nitro group (c).

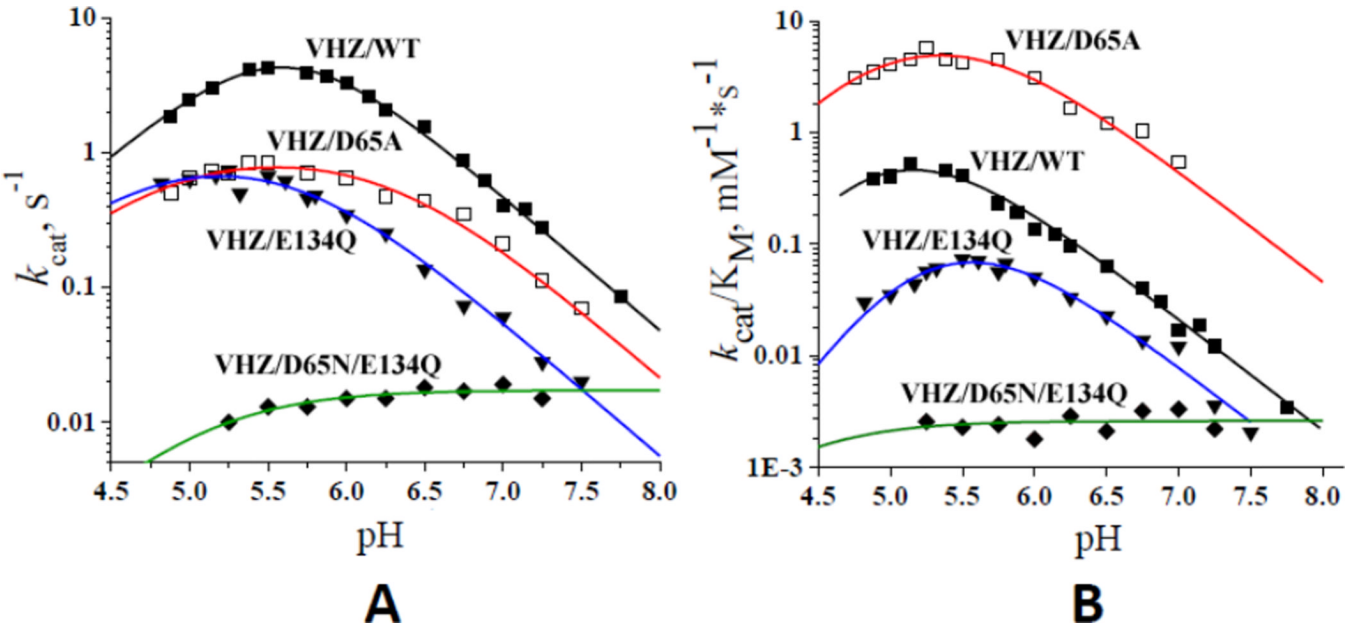

Figure 3.

pH rate profiles. A) k_{cat} for the native VHZ (black), D65A (red), and E143Q (blue), D65N/E134Q (green) mutants. B) k_{cat}/K_M for native VHZ, D65A, E134Q, D65N/E134Q mutants. The D65A mutant is more efficient than the native VHZ due to simultaneous reduction of k_{cat} and K_M. Both D65A and E134Q mutants retain the basic limb diagnostic of general acid catalysis. The basic limb completely disappears in VHZ/D65N/E134Q double mutant.

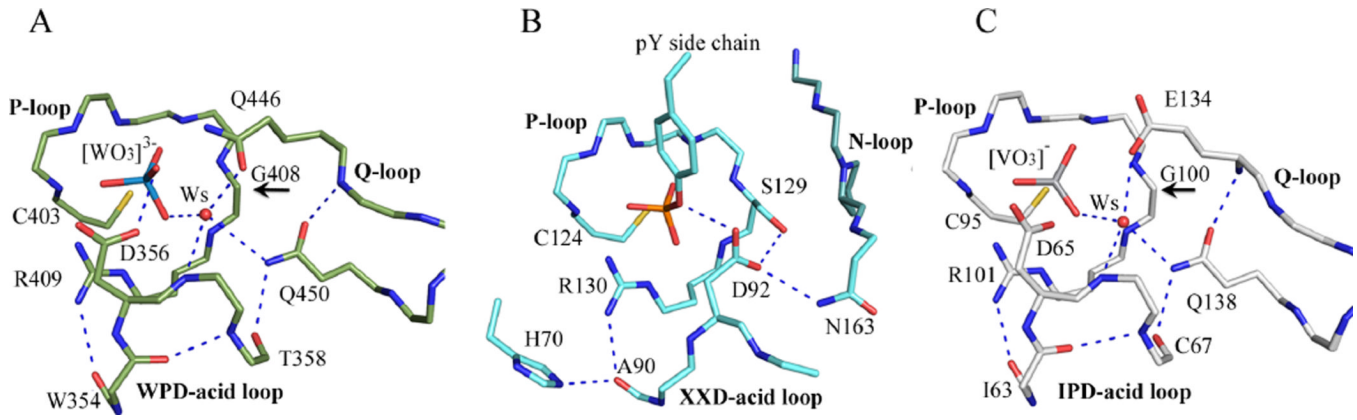

Figure 4.

Structural comparison of the active sites of: A) the PTP YopH; B) the DSP VHR; and C) VHZ. The structural arrangement of the VHR active site differs from YopH and VHZ in the replacement of the highly conserved Q-loop with the N-loop, and a different position of the general acid.

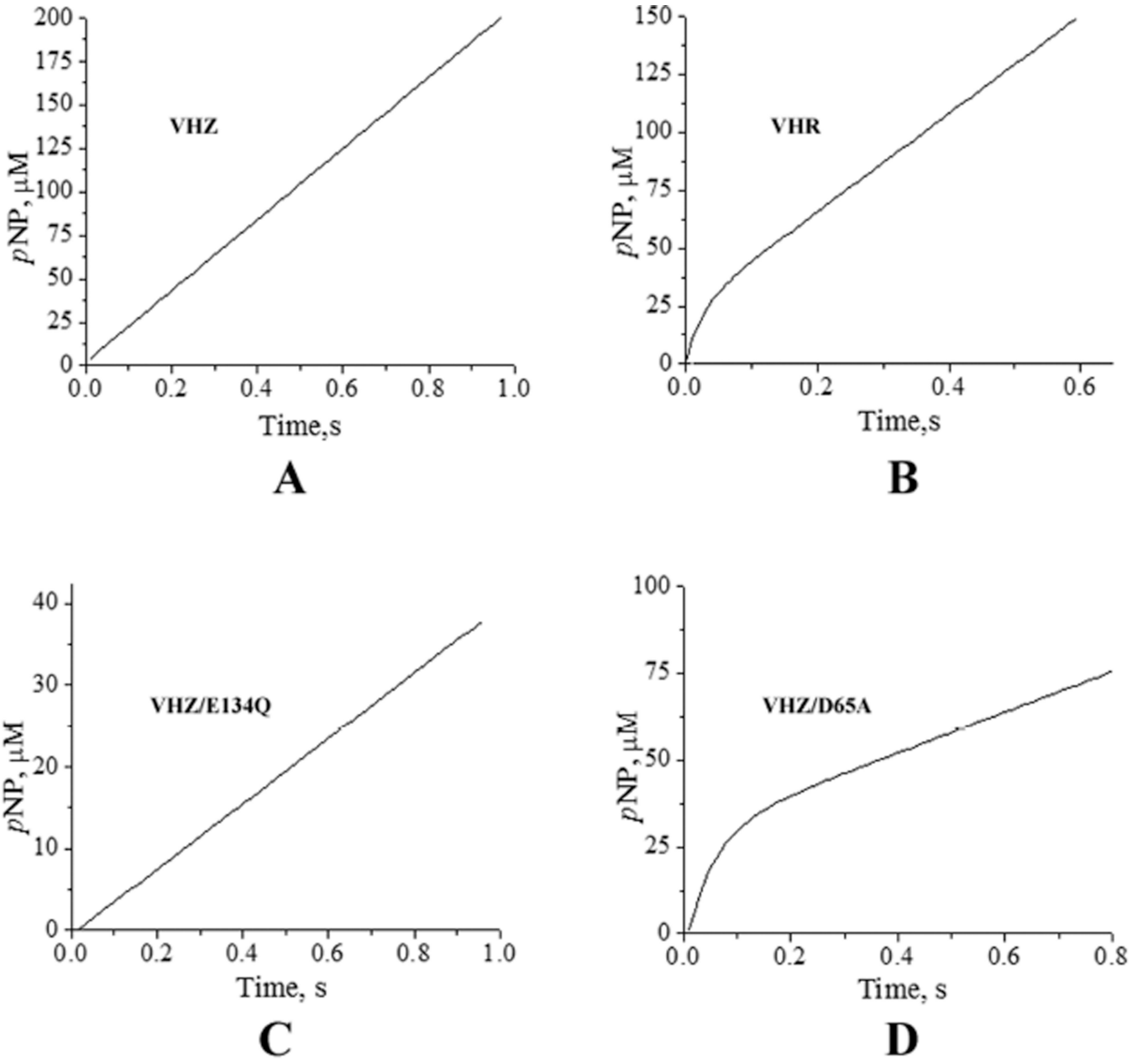

Figure 5.

Pre-steady state kinetics of: A) 48 μM native VHZ, with 50 mM *p*NPP; B) 26μM native VHR, with 50 mM *p*NPP; C) 58 μM VHZ/E134Q with 50 mM *p*NPP; D) 28 μM VHZ/D65A and 10 mM *p*NPP. All experiments were performed at 25 °C. 2000 data points were collected after 1ms mixing delay and used in the fit. Data points are omitted from the figure for clarity.

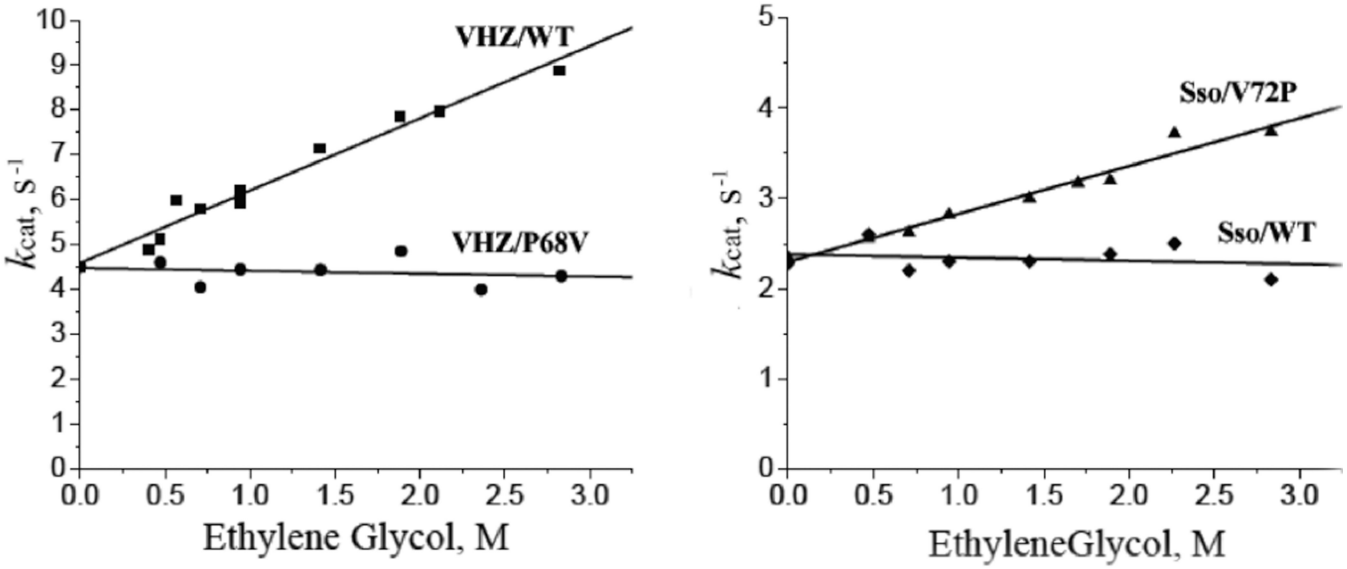

Figure 6.

Dependence of *p*NPP turnover on ethylene glycol concentration. A: VHZ /WT and VHZ/P68V mutant. B: SsoPTP/WT and Sso/V72P. The k_{cat} for *p*NPP release was plotted versus ethylene glycol concentration. All experiments were performed at 25°C.

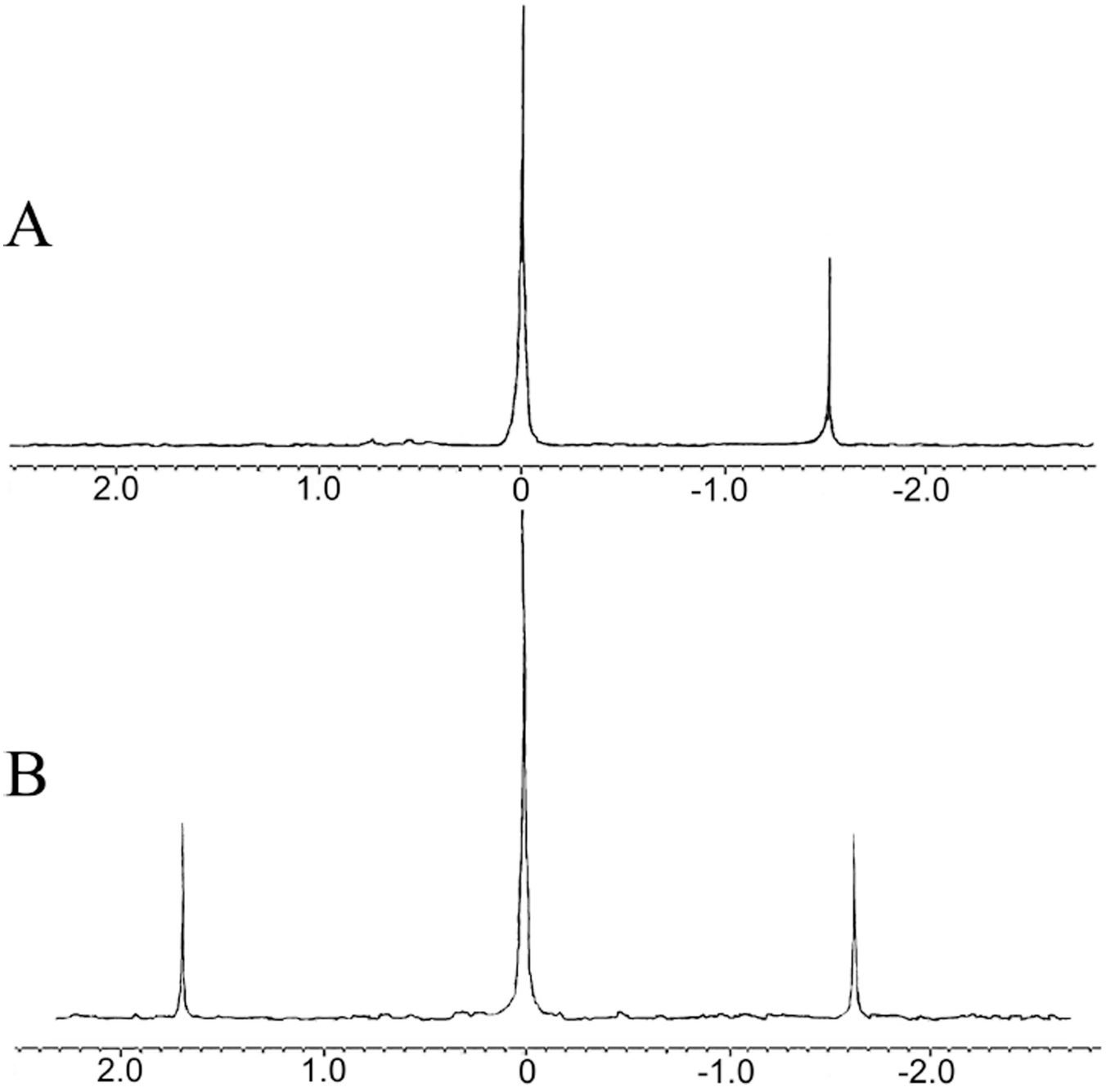

Figure 7.

Reaction of *p*NPP catalyzed by VHZ/P68V and VHZ monitored by ^{31}P NMR spectroscopy. Panel A shows the reaction of the VHZ/P68V mutant after 30 minutes in the presence of 1M Ethylene Glycol. Panel B shows the reaction catalyzed by VHZ after 30 minutes. All reactions were performed at pH 5.5 in 100 mM sodium acetate buffer in the presence of 20 mM *p*NPP. The chemical shift of *p*NPP was −1.6 ppm, inorganic phosphate was set to 0 ppm, and the shift of phosphorylated ethylene glycol is 1.7 ppm.

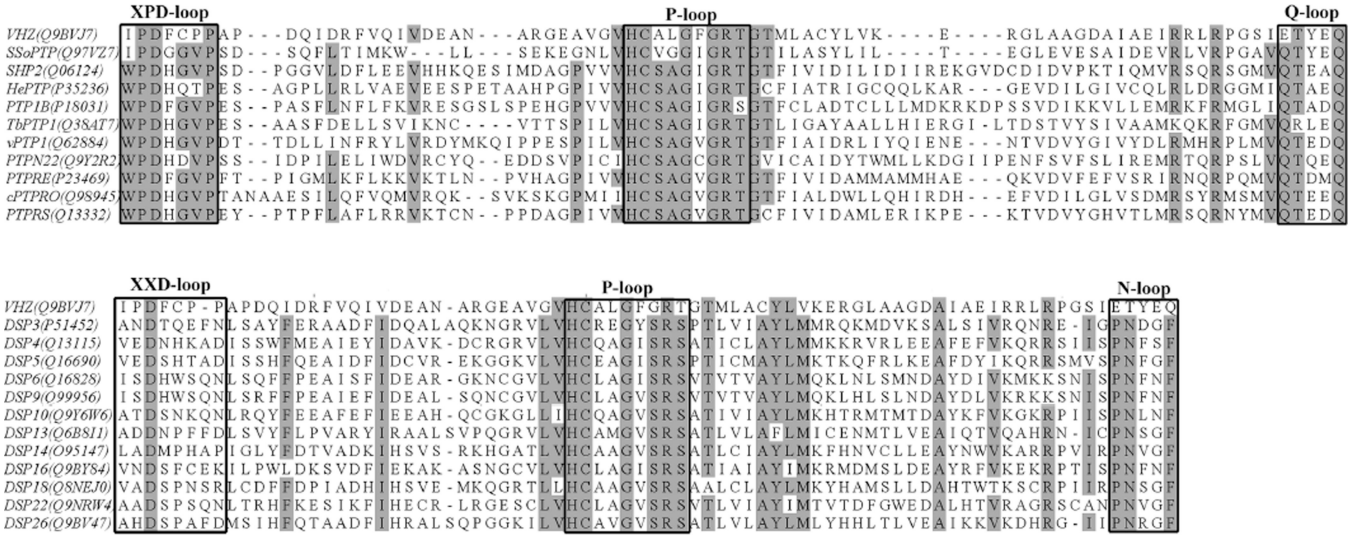

Figure 8.

Sequence alignment of residues 65–138 of VHZ with several classical PTPs (top) and atypical DSPs (bottom). The alignment is confined to the three catalytically important PTP regions, as they contain the highest sequence similarity in the PTP family. VHZ is more similar to classical PTPs than to the DSP family, with two important distinctions in the aligned regions: substitution of highly conserved W by I in the WPD-loop region; and; substitution of Q by E the Q-loop region.

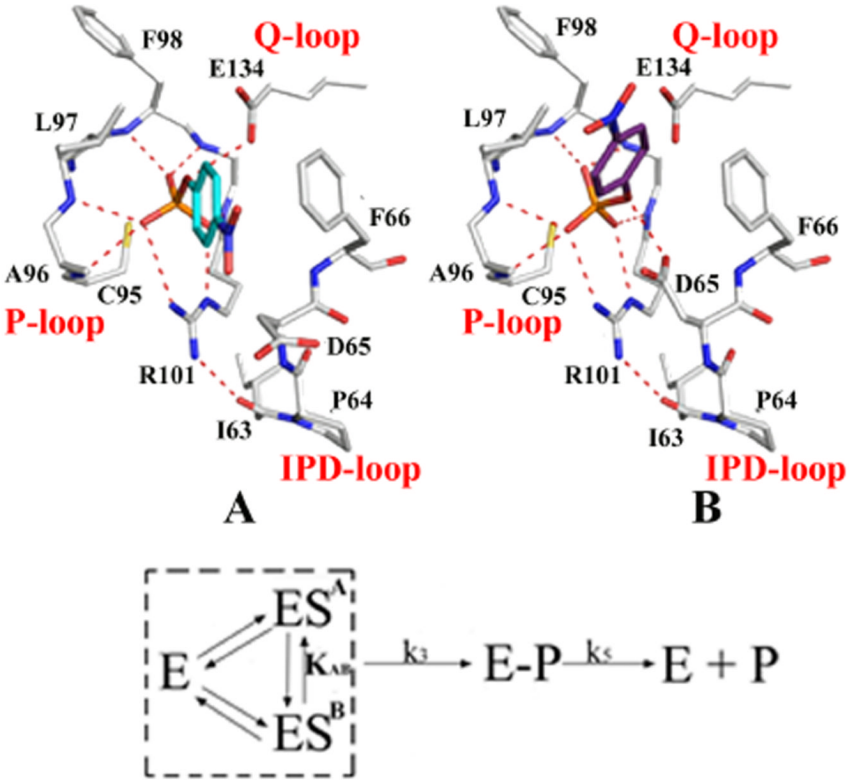

$$V_{max}^{A} + V_{max}^{B} = V_{max}^{WT} \times \alpha_A + V_{max}^{WT} \times \alpha_B = V_{max}^{WT} \times (\alpha_A + \alpha_B) = V_{max}^{WT} \times 1 = V_{max}^{WT}$$

Figure 9.

Two *p*NPP docking modes in the active site of VHZ predicted by docking studies. In mode A the scissile ester oxygen of the *p*NPP substrate is oriented towards the E134 side chain. Acid catalysis by D65 is unavailable, as its side chain is displaced to relieve a steric clash with the substrate. The D65A mutation removes this clash, explaining its lower K_M. When E134 is mutated, general acid catalysis by D65 can occur from the binding mode shown in B. Conformation B is analogous to that observed in the crystal structure of substrate bound to an inactive mutant of SsoPTP, and is consistent with the pH rate profile of E134Q.

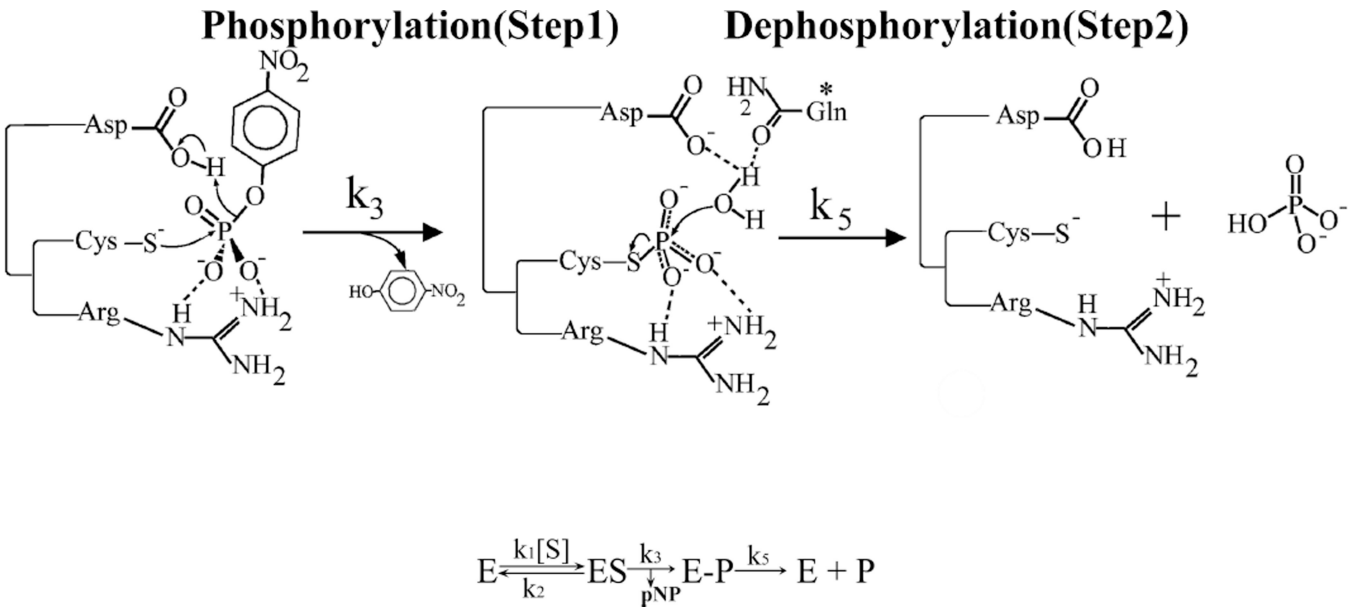

$$E \underset{k_2}{\overset{k_1[S]}{\rightleftharpoons}} ES \xrightarrow[pNP]{k_3} E\text{-}P \xrightarrow{k_5} E + P$$

Scheme 1.

Top, the chemical steps in the reaction catalyzed by PTPs. In the first chemical step a nucleophilic cysteine attacks the phosphate ester with simultaneous protonation of the leaving group by the conserved aspartic acid. In the second chemical step water attacks the phosphoenzyme intermediate liberating inorganic phosphate and free enzyme. Forward rate constants are numbered with odd subscripts, and reverse rate constants are shown with even subscripts. The Q-loop which is only present in classical PTPs serves to orient the incoming nucleophilic water and most commonly contains a catalytic glutamine residue marked with a star. This residue is represented by isosteric glutamic acid E134 in VHZ.

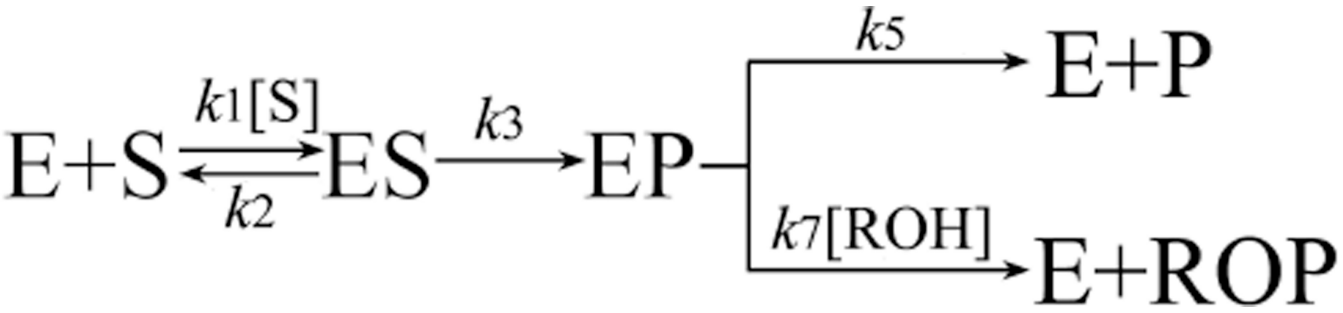

Scheme 2.
Partitioning of the enzyme-phosphate intermediate [E-P] between hydrolysis and alcoholysis pathways. Alcohols, or a water nucleophile, in two competing pathways attack the phosphoenzyme intermediate formed in the first step.

Table 1

Inhibition by buffers and oxyanions. Experiments were carried out at pH 5.5 in the 100 mM sodium acetate buffer where ionized form of tested buffering agents dominates in solution.

Compound	Inhibition Type	K_i, mM
Cyclohexylamine	Competitive	140 ± 10
EDTA	Competitive	22 ± 2
Inorganic phosphate		
VHZ/WT	Competitive	0.67 ± 0.05
VHZ/D65A	Competitive	0.43 ± 0.12
VHZ/D65N	Competitive	0.68 ± 0.11
Sso/WT	Competitive	0.54 ± 0.42
VHR/WT	Competitive	0.7 ± 0.3
YopH/WT	Competitive	4.4 ± 0.2
PTP1B/WT	Competitive	3.7 ± 0.1
Other oxyanions		
Sulfate	Competitive	4.6 ± 0.3
Arsenate	Competitive	0.13 ± 0.04
Vanadate	Competitive	0.0027 ± 0.0003
Buffers		
Tris	Competitive	88±9
N-ethyl morpholine NEM	No	No
Bis-Tris	Competitive	122±12
Triethanolamine	Competitive	52 ± 5
HEPES	Competitive	26 ± 3
Glycylglycine	Competitive	118 ± 12
Sodium acetate	No	No
Sodium succinate	No	No
3,3-demethylglutarate	No	No

Table 2

Kinetic isotope effects of native VHZ, PTP1B and VHR.

PTP name	$^{15}(V/K)$	$^{18}(V/K)_{bridge}$	$^{18}(V/K)_{non\text{-}bridge}$
VHZ	1.0013±0.0004	1.0164±0.0017	0.9986±0.0008
PTP1B (10)	1.0001±0.0002	1.0142 ± 0.0004	0.9981±0.0015
VHR (19)	0.9999±0.0004	1.0118±0.0020	1.0003±0.0003

Table 3

Kinetic data for native VHZ, YopH, VHR, PTP1B, and SsoPTP and selected mutants. Values are the results from at least six independent experiments.

Kinetic parameters with *p*NPP at pH 5.5 (optimum), 25°C			
	k_{cat},(s^{-1})	**K_M, mM**	**k_{cat}/K_M, $mM^{-1}s^{-1}$**
Native PTPs			
VHZ	3.92 ± 0.03	8.31 ± 0.71	0.47
VHR	3.1 ± 0.1	1.96 ± 0.11	1.59
SsoPTP	3.15 ± 0.05	4.31 ± 0.19	0.73
YopH	720 ± 25	0.98 ± 0.11	735
PTP1B	51.7 ± 0.9	0.12 ± 0.01	430
IPD- loop mutations			
Sso PTP/V72P	2.61 ± 0.1	4.62 ± 0.43	0.56
VHZ/D65A	0.84 ± 0.12	0.22 ± 0.01	4.19
VHZ/D65N	3.42 ± 0.12	8.73 ± 0.68	0.39
VHZ/D65N/E134Q	0.027 ± 0.002	27.77 ± 4.15	0.001
VHZ/P64A	0.07 ± 0.04	32.92 ± 2.98	0.002
VHZ/P69A	0.09 ± 0.05	31.00 ± 3.80	0.003
VHZ/P68V	3.34 ± 0.06	5.88 ± 0.27	0.57
Q-loop			
VHZ/E134Q	0.42 ± 0.07	7.66 ± 0.25	0.07
VHZ/E134A	0.29 ± 0.02	10.15 ± 1.32	0.03
VHZ/Q138A	0.13 ± 0.01	13.1 ± 1.7	0.01

Table 4

Elementary rate constants for *p*NPP hydrolysis and substrate dissociation constant for native VHR, VHZ/D65A, and native VHZ. The values for k_3, k_5 and K_S were obtained from burst kinetics as described in the SI. The kinetic constants for native VHZ were calculated based on the assumption that k_3 is not affected by the VHZ/D65A substitution, as described in the text. Under such circumstances, the system consisting of the two equations $k_{cat}=\frac{k_5 \times k_3}{k_3+k_5}$ and $K_M=K_S \times \frac{k_5}{k_3+k_5}$ can be solved to obtain values of k_5 and Ks.

	k_3,(s^{-1})	k_5,(s^{-1})	K_S, mM
VHZ/D65A	17.44 ± 0.13	1.71 ± 0.37	2.5
VHR	48.30 ± 0.34	9.70 ± 0.21	11.8
VHZ/WT	17.44 ± 0.13	5.19	35

Table 5

Second order rate constants for alcoholysis and hydrolysis of *p*NPP by several members of PTP family. The k_{cat} values obtained in the absence of alcohol (intercept with Y axis) were divided by the molarity of water (55.5 M) to yield the second order hydrolysis rate constant k_{cat}'. Nucleophilic specificity is defined by the relative preference for alcoholysis over hydrolysis. k_t corresponds to k_7 only when $k_5 >> k_3$, otherwise $k_t = \frac{k_3 \times k_7}{k_5 + k_3}$ (see SI for more detailed description). The values of k_t depend on the rate limiting step and on the overall activity, and should not be used to judge the preference for alcoholysis.

Name	k_t, $M^{-1}*sec^{-1}$	$k_{cat}'=(k_{cat}/55.5)$, $M^{-1}*sec^{-1}$	$S=k_t/k_{cat}'$
Ltp1/WT(7)	5.5	0.026	211.5
YopH/WT(6)	0.0	11.3	0.0
*SsoP*TP/WT	0.0	0.07	0.0
VHR/WT6)	0.48	0.07	6.85
VHZ/WT	1.3	0.09	14.4
VHZ/E134Q	0.06	0.005	12.1
VHZ/E134A	0.13	0.0036	36.1
YopH/Q446A(6)	21.6	1.11	19.4
VHZ/D65A	1.55	0.015	103.3
VHZ/P68V	0.0	0.060	0.0
SsoPTP/V72P	0.49	0.041	11.95